In summary, the electronic properties of the thallium ion in (P)TlM(L) lead to several specific properties of these bimetallic metal-metal-bonded complexes. Structural parameters show that the thallium metal ion is significantly more out of the porphyrin plane in (P)TlM(L) ($\Delta 4N$ = 0.939 (1) Å) than the indium metal ion in (P)InM(L)[9] ($\Delta 4N$ = 0.744 (1) Å), and this can explain the symmetry changes of the axial ligand noted by IR spectroscopy. The main differences between complexes in the (P)TlM(L) and the (P)InM(L) series are probably in the larger orbital overlap that occurs between the thallium atom and the axial metal. This results in a shorter metal-metal bond length and a greater stability of both the neutral and the singly or doubly oxidized (P)TlM(L) complexes. For the case of (P)TlMn(CO)$_5$ and (P)TlW(CO)$_3$Cp, this leads to well-defined reversible one- and two-electron oxidations.

Acknowledgment. The support of the CNRS, the National Science Foundation (Grant No. CHD-8515411 and No. INT-8413696), and the Robert A. Welch Foundation (Grant No. E-680) is gratefully acknowledged.

Registry No. (TPP)TlMn(CO)$_5$, 112022-35-2; (TPP)Co(CO)$_4$, 112022-36-3; (TPP)TlCr(CO)$_3$Cp, 112022-37-4; (TPP)TlMo(CO)$_3$Cp, 112022-38-5; (TPP)TlW(CO)$_3$Cp, 112022-39-6; (OEP)TlMn(CO)$_5$, 112041-61-9; (OEP)TlCo(CO)$_4$, 112041-62-0; (OEP)TlCr(CO)$_3$Cp, 112022-40-9; (OEP)TlMo(CO)$_3$Cp, 112022-41-0; (OEP)TlW(CO)$_3$Cp, 112041-63-1; (OEP)TlCl, 58167-68-3; (TPP)TlCl, 63848-51-1; [Cr(CO)$_3$Cp]Na, 12203-12-2; [Mo(CO)$_3$Cp]Na, 12107-35-6; [W(CO)$_3$Cp]Na, 12107-36-7; [Mn(CO)$_5$]Na, 13859-41-1; [Co(CO)$_4$]Na, 14878-28-5.

Supplementary Material Available: Tables of bond distances in angstroms, general displacement parameter expressions (B's), bond angles in degrees, and positional parameters and their estimated standard deviations (11 pages); a table of observed and calculated structure factors (36 pages). Ordering information is given on any current masthead page.

Contribution from the Department of Chemistry, Thimann Laboratories, University of California, Santa Cruz, California 95064, and Drug Dynamics Institute, College of Pharmacy, University of Texas, Austin, Texas 78712

Synthetic Analogue Approach to Metallobleomycins. 3. Synthesis, Crystal and Solution Structures, and Redox Properties of Bis(*N*-(2-(4-imidazolyl)ethyl)pyridine-2-carboxamido)cobalt(III) Perchlorate Hydrate

Karoline Delany, Satish K. Arora,† and Pradip K. Mascharak*

Received August 20, 1987

The cobalt(III) complex of PypepH (**1**), a peptide ligand resembling part of the metal-chelating portion of the antitumor drugs bleomycins (BLM), has been synthesized via aerobic oxidation of a mixture of **1** and cobalt(II) acetate (ratio 2:1) in aqueous or anhydrous methanol. [Co(Pypep)$_2$]ClO$_4$·H$_2$O (**2**) crystallizes in the trigonal space group $P3_121$ with a = 13.434 (3) Å, b = 13.434 (4) Å, c = 11.453 (3) Å, γ = 120.0°, and Z = 3. The structure was refined to R = 5.9% by using 2661 unique data ($F_o^2 > 2.5\sigma(F_o^2)$). The coordination geometry around low-spin Co(III) is octahedral with Co-N(pyridine) = 1.937 (5) Å, Co-N(imidazole) = 1.952 (5) Å, and Co-N(amido) = 1.933 (3) Å, respectively. Electrochemical reduction of **2** in DMF or methanol gives rise to an unstable Co(II) species that is rapidly converted into a high-spin octahedral Co(II) complex. The solution structure of [Co(Pypep)$_2$]$^+$ has been explored with the aid of one- and two-dimensional ^{1}H and ^{13}C NMR spectroscopy.

Introduction

Bleomycins (BLM), a family of glycopeptide antibiotics, induce extensive DNA damage in presence of metal ions like Fe^{2+} and molecular oxygen.[1-6] Clinical use of BLM in treatment of selected neoplastic diseases[6,7] is dependent on the DNA degradation reaction. Since cobalt(II) was reported to inactivate BLM,[8] initial interest in cobalt-bleomycin chelates (Co-BLMs) had been limited to some extent. Nevertheless, the coordination chemistry of Co-BLMs has been explored,[1-6,9-15] and Co-BLMs have found use in specific clinical applications. Co(III)-BLMs exhibit the unusual property of accumulating selectively in the nuclei of certain types of cancer cells, and radiolabeled kinetically inert ^{57}Co(III)-BLMs are used as diagnostic agents in nuclear medicine.[14] Recently, it has been reported that Co(III)-BLM can cause DNA strand breaks when irradiated with UV or visible light.[16-18] In both cases, cleavage of DNA is believed to be a consequence of photoreduction of Co(III)-BLM. This recently discovered bioactivity of Co(III)-BLM, namely, the photoinduced DNA damage by the metallodrug, has prompted renewed interest in the chemistry of Co-BLMs. As part of our "synthetic analogue approach"[19] to metallobleomycins (M-BLMs), we have underaken the task of looking into the structure of a few synthetic analogues of Co-BLMs. Previously we have reported the structures and spectral properties of Cu(II) complexes of two peptides resembling part of the metal-chelating region of BLM.[20] The low-spin Fe(III) complex of one of the peptides, *N*-(2-(4-imidazolyl)ethyl)-pyridine-2-carboxamide (**1**), has also been reported by us.[21] In

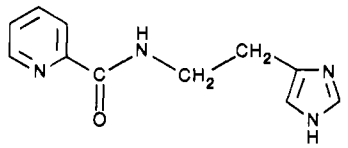

PypepH (1)

* To whom correspondence should be addressed at the University of California.
† To whom inquiries related to crystallographic data should be addressed at the University of Texas.

(1) Sugiura, Y.; Takita, T.; Umezawa, H. *Met. Ions Biol. Syst.* **1985**, *19*, 81.
(2) (a) Dabrowiak, J. C. *Adv. Inorg. Biochem.* **1983**, *4*, 69. (b) Dabrowiak, J. C. *Met. Ions Biol. Syst.* **1980**, *11*, 305. (c) Dabrowiak, J. C. *J. Inorg. Biochem.* **1980**, *13*, 317.
(3) Povrick, L. F. In *Molecular Aspects of Anticancer Drug Action*; Neidle, S., Waring, M. J., Eds.; Macmillan: London, 1983; p 157.
(4) Umezawa, H.; Takita, T. *Struct. Bonding (Berlin)* **1980**, *40*, 73.
(5) *Bleomycin: Chemical, Biochemical and Biological Aspects*; Hecht, S. M., Ed.; Springer-Verlag: New York, 1979.
(6) *Bleomycin: Current Status and New Developments*; Carter, S. K., Crooke, S. T., Umezawa, H., Eds.; Academic: New York, 1978.
(7) Blum, R. H.; Carter, S. K.; Agre, K. A. *Cancer (Philadelphia)* **1973**, *31*, 903.
(8) (a) Sausville, E. A.; Peisach, J.; Horwitz, S. B. *Biochemistry* **1978**, *17*, 2740. (b) Nagai, K.; Suzuki, H.; Tanaka, N.; Umezawa, H. *J. Antibiot.* **1969**, *22*, 569. (c) Nagai, K.; Yamaki, H.; Suzuki, H.; Tanaka, N.; Umezawa, H. *Biochim. Biophys. Acta* **1969**, *179*, 165.
(9) (a) Sugiura, Y. *J. Antibiot.* **1978**, *31*, 1206. (b) Sugiura, Y. *Biochem. Biophys. Res. Commun.* **1979**, *88*, 913. (c) Sugiura, Y. *J. Am. Chem. Soc.* **1980**, *102*, 5216.
(10) (a) Tsukayama, M.; Randall, C. R.; Santillo, F. S.; Dabrowiak, J. C. *J. Am. Chem. Soc.* **1981**, *103*, 458. (b) Dabrowiak, J. C.; Tsukayama, M. *J. Am. Chem. Soc.* **1981**, *103*, 7543.

0020-1669/88/1327-0705$01.50/0

this paper we report the synthesis, spectroscopic properties, and structure of the Co(III) complex of **1**. The solution structure of this synthetic analogue of Co(III)–BLM has also been elucidated by two-dimensional NMR work. Hereafter, the peptide is abbreviated as PypepH, the dissociable H being the amide H.

Experimental Section

Preparation of Compounds. PypepH (**1**) was synthesized by following the published procedure.[20] Cobalt(II) acetate tetrahydrate and cobalt carbonate were purchased from Alfa Products (Morton Thiokol Inc.). Lithium perchlorate, tetraethylammonium tetrafluoroborate, and cobalt chloride hexahydrate were procured from Aldrich Chemical Co. Crystalline cobalt(II) perchlorate hexahydrate was isolated from the pink solution obtained by dissolving cobalt carbonate in aqueous perchloric acid.

$[Co(Pypep)_2]ClO_4 \cdot H_2O$ (2). A 250-mg (1-mmol) amount of cobalt(II) acetate tetrahydrate was dissolved in 20 mL of 1:1 v/v mixture of water and methanol. The resulting pink solution was slowly added with stirring to a solution of 475 mg (2.2 mmol) of PypepH in 20 mL of the same solvent mixture. Within 5 min, the mixture assumed a deep red coloration. After 30 min, a batch of 212 mg (2 mmol) of $LiClO_4$ in 5 mL of methanol was added to the red mixture, and the clear deep red solution was stored at 0 °C for 72 h. The dark red crystals that separated during this period were collected by filtration, washed with cold water, and dried in air. A batch of 300 mg (yield 50%) of dark red blocks was obtained; mp 293–295 °C dec. Anal. Calcd for $C_{22}H_{24}N_8O_7CoCl$: C, 43.52; H, 3.99; N, 18.47; Cl, 5.84. Found: C, 43.61; H, 3.98; N, 18.53; Cl, 5.79. Presence of the single molecule of water was confirmed by X-ray crystallography and NMR spectroscopy (vide infra).

Addition of aqueous $LiClO_4$ to the deep red mixture of $Co(CH_3COO)_2 \cdot 4H_2O$ and PypepH (1:2.2 ratio) in water resulted in rapid precipitation of **2** as an orange solid. The solid was recrystallized from hot (~80 °C) water (yield 48%; mp 293–295 °C dec). The presence of water in these crystals was confirmed by NMR spectroscopy.

$[Co(Pypep)_2]ClO_4 \cdot CH_3OH$. When the reaction mentioned above was performed in anhydrous methanol, dark red blocks were isolated in 42% yield. These crystals contained one molecule of methanl per formula weight in the lattice. Anal. Calcd for $C_{23}H_{26}N_8O_7CoCl$: C, 44.47; H, 4.22; N, 18.05; Cl, 5.71. Found: C, 44.10; H, 4.17; N, 18.02; Cl, 5.70. The presence of methanol was also confirmed by NMR spectroscopy.

The IR spectrum of $[Co(Pypep)_2]ClO_4 \cdot H_2O$ is virtually identical with that of $[Co(Pypep)_2]ClO_4 \cdot CH_3OH$. Selected IR bands (KBr pellet, cm^{-1}): 3450 (m, br), 3200 (m, br), 1600 (ν_{CO}, vs), 1400 (m), 1240 (m), 1100 (ν_{ClO_4}, vs), 820 (w), 770 (m), 690 (m), 630 (m), 505 (w).

The tetrafluoroborate salt $[Co(Pypep)_2]BF_4 \cdot H_2O$ was isolated from a reaction mixture of $Co(CH_3COO)_2 \cdot 4H_2O$ and PypepH in aqueous methanol following addition of Et_4NBF_4. The tiny red crystals thus obtained were characterized by IR and absorption spectroscopy.

Table I. Summary of Crystal Data, Intensity Collection, and Structure Refinement Parameters for $[Co(Pypep)_2]ClO_4 \cdot H_2O$ (**2**)

formula (mol wt)	$C_{22}H_{24}N_8ClCoO_7$ (606.62)
a, Å	13.434 (3)
b, Å	13,434 (4)
c, Å	11.453 (3)
γ, deg	120.0
cryst syst	trigonal
V, Å^3	1790
Z	3
d_{calcd}, g/cm^3	1.688
d_{obsd},[a] g/cm^3	1.691 (5)
space group	$P3_121$
cryst dimens, mm	0.29 × 0.29 × 0.45
radiation (λ, Å)	Mo Kα (0.71069)
abs coeff (μ), cm^{-1}	10.19
scan speed, deg/min	6-12
2θ limits, deg	$4.0 < 2\theta < 55.0$
scan range, deg	symmetrically over 1.0 about $K\alpha_{1,2}$ max
bkgd/scan time ratio	1.0
no. of data collcd	8572 ($\pm h, \pm k, \pm l$)
no. of unique data ($F_o^2 > 2.5\sigma(F_o^2)$)	2661
no. of variables	210
goodness of fit	0.88
R,[b] %	5.9
R_w,[c] %	6.2
temp, K	163
transmissn factor range	0.77–0.79
largest residual electron density, e/Å^3	0.60 (assoc with O2)
max Δ/σ in final least-squares cycle	0.004

[a] Determined by flotation in $ZnCl_2/H_2O$. [b] $R = \sum||F_o| - |F_c||/\sum|F_o|$. [c] $R_w = [\sum w(|F_o| - |F_c|)^2/\sum w|F_o|^2]^{1/2}$; $w = 1/\sigma(|F_o|)^2$.

$[Co(Pypep)_2]^+$ from $CoCl_2$. A batch of 130 mg (1 mmol) of anhydrous $CoCl_2$[22] was dissolved in 15 mL of methanol, and the purple solution was filtered to remove trace of white residue. The filtrate was added with stirring to a solution of 450 mg (2.2 mmol) of PypepH in 15 mL of methanol. To the orange solution thus obtained was then added a methanolic solution (10 mL) of 170 mg (2 mmol) of sodium acetate. The color of the mixture rapidly changed to deep red. After 15 min of stirring, 212 mg (2 mmol) of $LiClO_4$ in 5 mL of methanol was added, and the clear red mixture was stored at 0 °C for 20 h. Dark red crystals of $[Co(Pypep)_2]ClO_4 \cdot CH_3OH$ (40% yield) were isolated by filtration, washed with ~5 mL of cold methanol, and dried in air.

A synthetic procedure similar to that described above but starting with $Co(ClO_4)_2 \cdot 6H_2O$ produced crystals of **2** in 45% yield. For the obvious reason, no $LiClO_4$ was used in this attempt.

Since $[Co(Pypep)_2]^+$ results from aerobic oxidation of some Co(II) species in solution (vide infra), mixing in all the cases described in this section was performed in open beakers to have ready access to air.

X-ray Data Collection and Reduction. Dark red blocks of $[Co(Pypep)_2]ClO_4 \cdot H_2O$ (**2**) were obtained from slow cooling of the reaction mixture in aqueous methanol. A suitable crystal was sealed in a glass capillary. Diffraction experiments were performed on a Syntex $P2_1$ diffractometer with graphite-monochromatized Mo Kα radiation and a Syntex LT-1 inert-gas (N_2) low-temperature delivery system. Data were obtained at 163 K. Machine parameters, crystal data, and data collection parameters are summarized in Table I. The orientation matrix and unit cell parameters were determined by using 35 machine-centered reflections in the region $23.1° \le 2\theta \le 29.8°$. Intensities of four check reflections were recorded after every 96 reflections to monitor crystal and instrument stability. Data were corrected for Lorentz and polarization effects, absorption, and decay.

Solution and Refinement of the Structure. Atomic coordinates for the Co atom were obtained by the direct-methods program MULTAN and confirmed by the Patterson method. The Co atom lies on a special position. The remaining non-hydrogen atoms were located from successive difference Fourier maps. The structure was refined by the least-squares method minimizing the function $\sum w(F_o - F_c)^2$ where $w = 1/\sigma(F_o)^2$. All non-hydrogen atoms were refined with anisotropic thermal parameters with appropriate constraints on atoms in special positions. Hydrogen atoms were located from difference Fourier maps, included in

(11) (a) Vos, C. M.; Westera, G.; van Zanten, B. *J. Inorg. Biochem.* **1980**, *12*, 45. (b) Vos, C. M.; Westera, G.; Schipper, D. *J. Inorg. Biochem.* **1980**, *13*, 165. (c) Vos, C. M.; Westera, G. *J. Inorg. Biochem.* **1981**, *15*, 253.
(12) (a) Sugiura, Y.; Suzuki, T.; Otsuka, M.; Kobayashi, S.; Ohno, M.; Takita, T.; Umezawa, H. *J. Biol. Chem.* **1983**, *258*, 1328. (b) Umezawa, H.; Takita, T.; Sugiura, Y.; Otsuka, M.; Kobayashi, S.; Ohno, M. *Tetrahedron* **1984**, *40*, 501.
(13) (a) Garnier-Suillerot, A.; Albertini, J. P.; Tosi, L. *Biochem. Biophys. Res. Commun.* **1981**, *102*, 499. (b) Albertini, J. P.; Garnier-Suillerot, A. *Biochemistry* **1982**, *21*, 6777.
(14) (a) Rasker, J. J.; Van de Poll, M. A. P. C.; Beekhins, H.; Woldring, M. G.; Nieweg, H. O. *J. Nucl. Med.* **1975**, *16*, 1058. (b) Nouel, J. P. *Gann Monogr. Cancer Res.* **1976**, *19*, 301. (c) Nunn, A. D. *Int. J. Nucl. Med. Biol.* **1977**, *4*, 204. (d) Kono, A.; Matsushima, Y.; Kojima, M.; Maeda, T. *Chem. Pharm. Bull.* **1977**, *25*, 1725. (e) DeRiemer, L. H.; Meares, C. F.; Goodwin, D. A.; Diamanti, C. I. *J. Med. Chem.* **1979**, *22*, 1019. (f) Raban, P.; Brousil, J.; Svikovcova, P. *Eur. J. Nucl. Med.* **1979**, *4*, 191. (g) Kakinuma, J.; Kagiyama, R.; Orii, H. *Eur. J. Nucl. Med.* **1980**, *5*, 159.
(15) Chang, C.-H.; Dallas, J. L.; Meares, C. F. *Biochem. Biophys. Res. Commun.* **1983**, *110*, 959.
(16) (a) Chang, C.-H.; Meares, C. F. *Biochemistry* **1982**, *21*, 6332. (b) Chang, C.-H.; Meares, C. F. *Biochemistry* **1984**, *23*, 2268.
(17) (a) Suzuki, T.; Kuwahara, J.; Sugiura, Y. *Nucleic. Acids Res.* **1984**, *15*, 161. (b) Suzuki, T.; Kuwahara, J.; Goto, M.; Sugiura, Y. *Biochim. Biophys. Acta* **1985**, *824*, 330.
(18) Subramanian, R.; Meares, C. F. *J. Am. Chem. Soc.* **1986**, *108*, 6427.
(19) Ibers, J. A.; Holm, R. H. *Science (Washington, D.C.)* **1980**, *209*, 223.
(20) Brown, S. J.; Tao, X.; Stephan, D. W.; Mascharak, P. K. *Inorg. Chem.* **1986**, *25*, 3377.
(21) Tao, X.; Stephan, D. W.; Mascharak, P. K. *Inorg. Chem.* **1987**, *26*, 754.

(22) Deep blue powder of anhydrous $CoCl_2$ was obtained by heating (80 °C) $CoCl_2 \cdot 6H_2O$ under vacuum for 48 h.

Table II. Positional Parameters ($\times 10^4$) for $[Co(Pypep)_2]ClO_4 \cdot H_2O$ (2)

atom	x	y	z
Co	10000 (0)	4006 (1)	6666 (0)
O1	8769 (3)	2385 (3)	9723 (3)
N1	9033 (3)	4540 (3)	5949 (3)
N2	8194 (4)	5103 (4)	4680 (4)
N3	9049 (3)	3464 (3)	8048 (3)
N4	10821 (3)	3339 (4)	7420 (3)
C1	8282 (4)	4783 (4)	6537 (4)
C2	7756 (5)	5123 (5)	5747 (5)
C3	8961 (4)	4751 (4)	4830 (4)
C4	8162 (5)	4677 (5)	7831 (4)
C5	8036 (5)	3565 (5)	8298 (5)
C6	9290 (4)	2859 (4)	8797 (4)
C7	10289 (5)	2746 (4)	8400 (4)
C8	10597 (5)	2019 (5)	8936 (5)
C9	11474 (6)	1886 (6)	8431 (5)
C10	12013 (5)	2487 (5)	7441 (5)
C11	11671 (5)	3218 (5)	6963 (5)
Cl	4544 (12)	4539 (12)	5000 (0)
O2	5347 (7)	4824 (14)	4162 (7)
O3	4370 (7)	3564 (5)	5573 (5)
OW	10000 (0)	2305 (4)	11666 (0)

Table III. Selected Bond Distances and Angles for $[Co(Pypep)_2]^+$

	Distances (Å)		
Co–N1	1.952 (5)	C5–N3	1.462 (9)
Co–N3	1.933 (3)	N3–C6	1.328 (7)
Co–N4	1.937 (5)	C6–C7	1.495 (9)
C1–N1	1.381 (7)	C6–O1	1.253 (5)
C1–C2	1.360 (8)	C7–N4	1.355 (6)
C1–C4	1.490 (6)	C7–C8	1.381 (10)
C2–N2	1.362 (8)	C8–C9	1.402 (11)
N2–C3	1.343 (9)	C9–C10	1.370 (8)
C3–N1	1.327 (6)	C10–C11	1.388 (11)
C4–C5	1.514 (9)	C11–N4	1.338 (9)
	Angles (deg)		
N1–Co–N3	92.7 (2)	Co–N3–C6	116.2 (4)
N1–Co–N4	174.3 (3)	C5–N3–C6	117.0 (4)
N3–Co–N4	83.3 (2)	N3–C6–O1	127.6 (4)
Co–N1–C1	125.5 (4)	N3–C6–C7	111.8 (4)
Co–N1–C3	128.2 (4)	O1–C6–C7	120.5 (4)
C1–N1–C3	106.3 (4)	C6–C7–N4	115.4 (4)
N1–C1–C2	108.6 (4)	C6–C7–C8	122.6 (5)
N1–C1–C4	121.3 (4)	N4–C7–C8	121.8 (5)
C2–C1–C4	130.1 (4)	Co–N4–C7	112.7 (4)
C1–C2–N2	107.9 (6)	Co–N4–C11	125.8 (4)
C2–N2–C3	108.0 (4)	C7–N4–C11	119.7 (4)
N2–C3–N1	110.5 (4)	C7–C8–C9	118.4 (5)
C1–C4–C5	113.5 (4)	C8–C9–C10	119.8 (6)
C4–C5–N3	111.9 (5)	C9–C10–C11	116.8 (5)
Co–N3–C5	126.6 (4)	C10–C11–N4	122.4 (5)

the model but not refined. A total of 2661 unique data ($F_o^2 > 2.5\sigma(F_o^2)$) was used in the refinement. The final R factors are included in Table I. Non-hydrogen atomic scattering factors were taken from literature tabulations.[23] Atomic positional parameters are listed in Table II. Selected bond distances and angles are presented in Table III. Thermal parameters of cation and anion (Table S1), bond distances and angles for the anion (Table S2), positional parameters for hydrogen atoms (Table S3), unweighted least-squares planes of the cation (Table S4), and the values of $10|F_o|$ and $10|F_c|$ (Table S5) are deposited as supplementary material.

Other Physical Measurements. Absorption spectra were obtained with a Perkin-Elmer Lambda 9 spectrophotometer. Infrared spectra were measured on a Nicolet MX-S FTIR spectrometer. ^1H and ^{13}C NMR spectra were recorded on a General Electric 300-MHz GN-300 instrument. Samples were dissolved in $(CD_3)_2SO$ (99% D). Multiplicities of ^{13}C NMR peaks were determined from APT or DEPT data. EPR spectra were recorded on a Varian E-3 spectrometer connected to a Digital PDP 11 computer for data manipulation. Electrochemical measurements were performed with standard Princeton Applied Research instrumentation using a Pt or glassy-carbon electrode; potentials were measured at ~25 °C vs. a saturated calomel electrode as reference. Elemental analyses were completed by Atlantic Microlab Inc., Atlanta, GA.

Two-Dimensional NMR Procedures. Standard pulse sequences[24] were used to obtain ^1H–^1H and ^1H–^{13}C two-dimensional scalar-correlated NMR spectra. For ^1H–^1H COSY, the spectral acquisition parameters were 4167 Hz in both F_2 and F_1 dimensions with a relaxation pulse delay of 100 ms. A total of 512 evolution increments of 240 μs each were employed beginning at an initial delay period of 10 μs. Apodization by a sine function was employed in each dimension. For ^1H–^{13}C COSY, the spectral parameters were 12 500 Hz in the F_2 dimension and 4167 Hz in F_1 with a relaxation pulse delay of 1 s. A total of 128 evolution increments were employed. The initial delay period in this case was also 10 μ. The original 1024 × 128 data matrix was zero filled and then transformed into a 1024 × 256 matrix. A double exponential multiplication function was used for apodization in each dimension. Detection of correlations (normal range, J = 140 Hz) was facilitated by utilizing the delay $\tau_1 = 0.5/J$ preceding the polarization transfer pulse and a refocusing delay $\tau_2 = 0.3/J$ with τ values respectively of 3.5 and 2.0 ms. In the case of long-range correlation (J = 9 Hz), the τ values were 55.6 and 33.3 ms, respectively.

Results and Discussion

Oxygenation of solutions containing Co(II) and N-donor ligands often results in complicated consecutive reactions that eventually yield Co(III) compounds along with superoxo and binuclear peroxo complexes.[25] In spite of this complication, the majority of the peptide complexes of tervalent cobalt has been synthesized by following the oxygenation procedure.[26,27] The present work is no exception; the Co(III) complex of the peptide ligand **1** has also been synthesized by aerobic oxidation of mixtures of Co(II) salts and **1** in anhydrous or aqueous methanol. Presence of a base like sodium acetate or hydroxide[28] is required in such mixtures. Like other peptide complexes,[27] deprotonation of the amide hydrogen and concomitant coordination of the amido N to cobalt appear essential for the oxygenation step. Cobalt(II) acetate tetrahydrate is the most suitable starting material. When cobalt(II) chloride or perchlorate is used, 2 equiv of sodium acetate (or hydroxide) is needed for the facile formation of $[Co(Pypep)_2]^+$. Aeration of a mixture of $CoCl_2$ and 2 equiv of **1** in anhydrous methanol results in an orange red solution that exhibits a complicted absorption spectrum. When $LiClO_4$ is added to this solution, a sticky off-white solid separates out. Addition of 2 equiv of sodium acetate to this heterogeneous mixture, however, brings about rapid dissolution of the off-white solid and appearance of the characteristic deep red coloration due to $[Co(Pypep)_2]^+$. On cooling, crystals of $[Co(Pypep)_2]ClO_4 \cdot CH_3OH$ are deposited from this red solution. Interestingly, in the absence of a base, a moderate amount of water in the reaction mixture leads to partial formation of $[Co(Pypep)_2]^+$. When a mixture of 2 equiv of **1** and 1 equiv of $CoCl_2 \cdot 6H_2O$ or $Co(ClO_4)_2 \cdot 6H_2O$ in aqueous methanol is stirred in air, the color first changes to deep brown (indicating formation of oxygenated complex) and then gradually turns red-brown within a few hours.[29] So far we have been unsuccessful in isolating any crystalline product from such solutions. Clearly, the presence of a base accelerates the formation of $[Co(Pypep)_2]^+$ and makes isolation of the desired product possible. It is, however, important to note that no intermediate brown coloration is observed during aeration of reaction mixtures containing acetate.

That oxygen is the oxidizing agent in the syntheses described above has also been confirmed. Under strictly anaerobic conditions, addition of 1 equiv of cobalt(II) acetate tetrahydrate to 2.2 equiv of **1** in methanol produces an orange solution (vide infra) that remains unchanged for hours when kept under argon. When

(23) Cromer, D. T.; Weber, J. T. *International Tables for X-ray Crystallography*; Kynoch: Birmingham, England, 1974; Vol. IV.
(24) Benn, R.; Gunther, H. *Angew. Chem., Int. Ed. Engl.* **1983**, *48*, 350.
(25) Cotton, F. A.; Wilkinson, G. In *Advanced Inorganic Chemistry*, 4th ed.; Wiley: New York, 1980; pp 776–778.
(26) Boas, L. V.; Evans, C. A.; Gillard, R. D.; Mitchell, P. R.; Phipps, D. A. *J. Chem. Soc., Dalton Trans.* **1979**, 582.
(27) Sundberg, R. J.; Martin, R. B. *Chem. Rev.* **1974**, *74*, 471.
(28) Triethylamine works quite as well.
(29) Electronic absorption spectrum of the red-brown solution exhibits the 495-nm band due to $[Co(Pypep)_2]^+$. However, this band is broader as compared to one exhibited by an authentic sample of **2**. Also, there are other differences in the high-energy regions of the spectra.

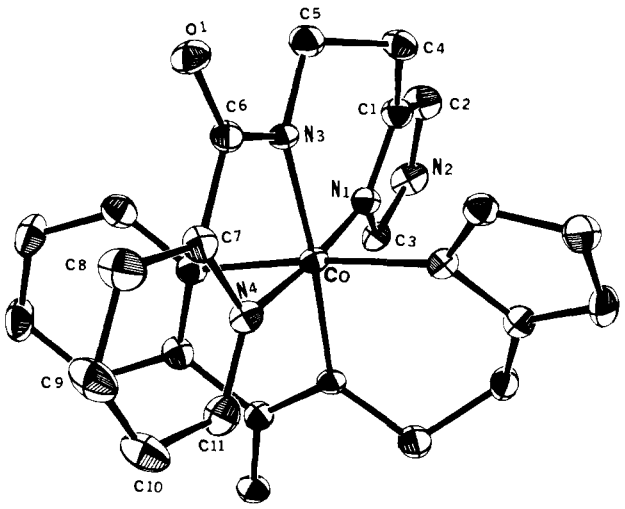

Figure 1. ORTEP drawing of $[Co(Pypep)_2]^+$ showing 50% probability ellipsoids and the atom-labeling scheme. Hydrogen atoms have been omitted for clarity.

this solution is exposed to air and stirred, deep red swirls are seen and soon a dark red solution of $[Co(Pypep)_2]^+$ is obtained. Spin-trapping experiments[30] with the orange solution during various stages of oxygenation, however, showed very weak signals due to superoxide radical. This result is not surprising since neither superoxide nor peroxide has been found in required amounts in oxygenation reactions leading to Co(III) complexes of peptides.[27]

Structure of $[Co(Pypep)_2]ClO_4 \cdot H_2O$ (2). The crystal structure is made up of discrete cations and anions. The Co atom of the cation sits on a special position. The closest approach of two cations is 2.892 Å (O1–N2) through hydrogen bonding. Additional hydrogen bonding between O1 and the oxygen atom of the water molecule is evidenced by the O1–O(water) distance of 2.806 Å.

An ORTEP drawing of the cation is shown in Figure 1. The coordination geometry around the cobalt atom is octahedral. The tridentate anionic ligand is bonded to cobalt with the pyridine and imidazole N atoms being trans to one another. The two deprotonated amido N atoms are also trans to each other. Thus the isolated complex is the *mer* isomer. The Fe(III) complex $[Fe(Pypep)_2]Cl \cdot 2H_2O$[21] has also been isolated as the *mer* isomer.

Selected interatomic distances and angles for **2** are listed in Table III. The Co(III)–N_{py} (py = pyridine) distance of 1.937 (5) Å is close to the mean Co(III)–N_{py} distance (1.945 (5) Å) found in $[Co(en)(2\text{-}AMP)_2]^{3+}$ where 2-AMP is the bidentate 2-(aminoethyl)pyridine ligand.[31] The average Co(III)–N_{py} distance in $[Co(CO_3)(py)_4]ClO_4 \cdot H_2O$ is, however, considerably longer (1.989 (5) Å),[32] and this is also true for the case with $[CoBr(en)_2py](NO_3)_2$,[33] where the Co(III)–N_{py} bond is 2.016 (26) Å long. Apparently, formation of a five-membered chelate ring has brought the pyridine N atoms closer to the cobalt atom in **2**. The Co(III)–N_{im} (im = imidazole) distance in **2** (1.952 (5) Å) is comparable to that observed in histidinato (His) complexes like $[Co(NO_2)(L\text{-}His)_2] \cdot H_2O$ (1.958 (10) Å)[34] and [Co(en)Cl(His)]Cl (1.946 (3) Å).[35,36] The Co(III)-N (amido) bond in **2** is 1.933 (3) Å long. Similar lengths for the Co(III)–N (amido) bond have been reported with $(NH_4)[Co(gly\text{-}gly)_2] \cdot 2H_2O$ (1.92 Å),[40] $[Co(H_2O)_6][Co(gly\text{-}gly)_2]_2 \cdot 12H_2O$ (1.87 Å),[41] and $[Co(NH_3)_2(L\text{-}ala\text{-}gly\text{-}gly)]$ (1.869 (6) Å).[42] The Cl atom of the anion lies on a 2-fold axis and the Cl–O distances (1.362 (14) Å, mean) as well as the O–Cl–O angle (109.9°) appear to be rather normal.[32]

The angles around cobalt that show maximum deviation from 90° are the N(amido)–Co–N_{py} angles. Formation of a five-membered chelate ring with extended conjugation only allows a N(amido)–Co–N_{py} angle of 83.3 (2)° instead of 90°. In $Fe(Pypep)_2]^+$, the corresponding angles are even smaller (81°). The oversized N(amido)–Co–N_{im} angle (92.7 (2)°), on the other hand, is the natural result of a six-membered chelate ring possessing flexible $-CH_2-$ linkers between the amido N and imidazole. The trans N atoms around cobalt (Figure 1) are drawn to each other to some extent such that the N–Co–N angles are close to 174°.

Table IV. Spectroscopic and Electrochemical Data for $[Co(Pypep)_2]^+$

solvent	λ_{max}, nm (ϵ, M^{-1} cm^{-1})	$E_{1/2}$,[a] V
MeOH	495 (210), 320 (3900), 258 (12 700)	−0.62
Me_2SO	500 (230), 330 (4000), 262 (14 000)	−0.70
DMF	503 (210), 330 (4000)	−0.69[b]
MeCN	503 (210), 330 (3700), 262 (12 500)	

[a] Cyclic voltammetry, glassy-carbon electrode, 0.1 M tetrabutylammonium perchlorate as supporting electrolyte, 100 mV/s scan speed. Values quoted vs aqueous SCE. [b] With tetraethylammonium tetrafluoroborate (0.1 M) as supporting electrolyte, the $E_{1/2}$ value is −0.70 V (Figure 3).

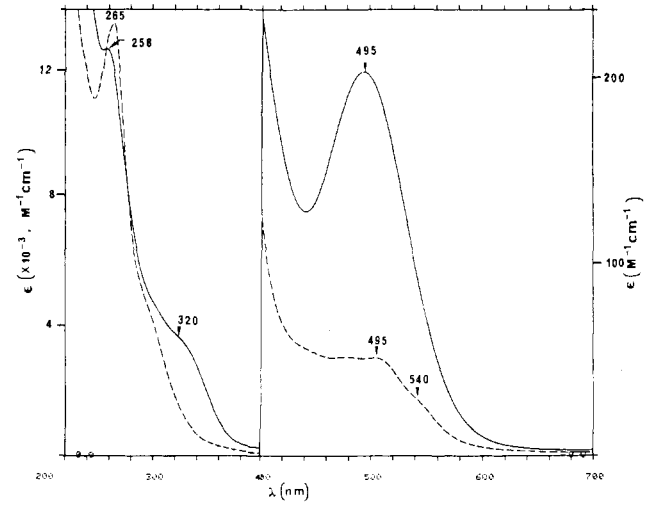

Figure 2. Absorption spectrum of $[Co(Pypep)_2]ClO_4 \cdot H_2O$ (**2**) in methanol (solid line). The 700–200-nm portion of the absorption spectrum of the Co(II) complex from the reaction between **1** and cobalt(II) acetate is degassed methanol is shown by the broken line. The latter species displays one more band with a maximum at 1040 nm (ϵ = 8 M^{-1} cm^{-1}).

Properties. (a) Electronic Spectra. Orange to orange-red solutions of $[Co(Pypep)_2]^+$ exhibit three bands with maxima at ~500, ~330, and ~260 nm (Figure 2, Table IV). For low-spin octahedral Co(III), two d–d transitions, namely $^1A_{1g} \rightarrow {}^1T_{1g}$ and $^1A_{1g} \rightarrow {}^1T_{2g}$ are expected. Complexes containing the $Co^{III}N_6$

(30) The spin-trapping experiments were performed with *N-tert*-butyl-α-phenylnitrone (PBN) as the spin trap. Instrument settings: frequency, 9.129 GHz; modulation frequency, 100 KHz; modulation amplitude, 1 G; power, 10 mW; gain, 1×10^5; temperature, 10 °C. The concentration of cobalt was 1 mM. Samples were prepared by bubbling O_2 through the cobalt solution for 20, 40, 60, 80, 100, and 120 s in presence of the spin trap.

(31) Sekizaki, M.; Utsuno, S. *Bull. Chem. Soc. Jpn.* **1979**, *52*, 3302.
(32) Kaas, K.; Sorensen, A. M. *Acta Crystallogr., Sect. B: Struct. Crystallogr. Cryst. Chem.* **1973**, *B29*, 113.
(33) Bortin, O. *Acta Chem. Scand., Ser. A* **1976**, *A30*, 475.
(34) Herak, R.; Prelesnik, B.; Kamberi, B.; Celap, M. B. *Acta Crystallogr., Sect. B: Struct. Crystallogr. Cryst. Chem.* **1981**, *B37*, 1989.
(35) Brodsky, N. R.; Nguyen, N. M.; Rowan, N. S.; Storm, C. B.; Butcher, R. J.; Sinn, E. *Inorg. Chem.* **1984**, *23*, 891.
(36) Considerably shorter Co(III)–N_{im} distances are observed in $[Co(L\text{-}His)_2]ClO_4 \cdot 2H_2O$ (1.923 (6) Å, mean),[37] [Co(L-His)(D-Pen)]·H_2O (1.925 (3) Å; D-Pen = D-penicilliaminato),[38] and [Co(L-OHBH)(ala)]·$2H_2O$ (1.917 (6) Å), L-OHBA = N^{α}-(*o*-hydroxybenzyl)-L-histidinato, ala = L-alaninato).[39]
(37) Thorup, N. *Acta Chem. Scand., Ser. A* **1979**, *A33*, 759.
(38) Meester, P.; Hodgson, D. J. *J. Am. Chem. Soc.* **1977**, *99*, 101.
(39) Voss, K. E.; Angelici, R. J.; Jacobson, R. A. *Inorg. Chem.* **1978**, *17*, 1922.
(40) Gillard, R. D.; Mckenzie, E. D.; Mason, R.; Robertson, G. B. *Nature (London)* **1966**, *209*, 1347.
(41) Barnet, M. T.; Freeman, H. C.; Buckingham, D. A.; Hsu, I.; van der Helm, D. *J. Chem. Soc., Chem. Commun.* **1970**, 367.
(42) Evans, J. E.; Hawkins, C. J.; Rodgers, J.; Snow, M. R. *Inorg. Chem.* **1983**, *22*, 34.

chromophore typically have an absorption in the region 450–500 nm ($\epsilon \sim 10$–$300\ M^{-1}\ cm^{-1}$) corresponding to the $^1A_{1g} \rightarrow {}^1T_{1g}$ transition.[43] In peptide complexes of Co(III) with the $Co^{III}N_4O_2$ chromophore, the same transition gives rise to a band at ~520 nm ($\epsilon \sim 250$–$400\ M^{-1}\ cm^{-1}$).[26,42,44] We assign the ~500-nm band of $[Co(Pypep)_2]^+$ to the $^1A_{1g} \rightarrow {}^1T_{1g}$ transition. In most Co(III) complexes of high symmetry, the two d–d transitions give rise to absorption bands of nearly equal intensity.[43] The peptide complexes of Co(III), however, show a less intense ($\epsilon \sim 100\ M^{-1}\ cm^{-1}$) band in the 390–400-nm region due to the $^1A_{1g} \rightarrow {}^1T_{2g}$ transition.[26] In case of $[Co(Pypep)_2]^+$, the second band at ~330 nm (Table IV) is unusually strong ($\epsilon \sim 4000\ M^{-1}\ cm^{-1}$) and presumably arises from charge-transfer (CT) absorption. It is quite possible that the $^1A_{1g} \rightarrow {}^1T_{2g}$ transition is hidden under this intense band. With $[Fe(Pypep)_2]^+$, a ligand-to-metal charge-transfer (LMCT) band of nearly identical intensity has been recorded at ~365 nm.[21] Since the LMCT process involves transfer of an electron from L to the e_g level of $Co^{3+}(d^6)$ as opposed to a t_{2g} level in the case of $Fe^{3+}(d^5)$,[45] a blue shift of the LMCT band is expected as one goes from $[Fe(Pypep)_2]^+$ to $[Co(Pypep)_2]^+$. This is indeed what is observed; therefore, the ~330-nm band of $[Co(Pypep)_2]^+$ is assumed to be a LMCT band. Interestingly, the Co(III) complex of the pseudotetrapeptide A of BLM[10] exhibits an even more intense absorption ($\epsilon = 6500\ M^{-1}\ cm^{-1}$) with λ_{max} at 324 nm, which has also been suggested to have a CT origin. The third band exhibited by $[Co(Pypep)_2]^+$ at ~260 nm arises from absorption by the organic chromophore of the peptide ligand.[46]

Under anaerobic conditions, addition of cobalt(II) acetate tetrahydrate to 2.1 equiv of **1** in anhydrous methanol results in a pale orange solution. The electronic spectrum of this orange solution displays absorption maxima at 1040 ($\epsilon = 8\ M^{-1}\ cm^{-1}$), 540 ($\epsilon = 30\ M^{-1}\ cm^{-1}$), 495 ($\epsilon = 50\ M^{-1}\ cm^{-1}$), and 265 ($\epsilon = 13\,000\ M^{-1}\ cm^{-1}$) nm (Figure 2), typical of octahedral high-spin Co(II) complexes.[44,47] Also, the orange solution exhibits no EPR spectrum at liquid-nitrogen temperature. With high-spin d^7 systems in the octahedral crystal field, spin–orbit coupling allows EPR measurements only at very low temperatures.[48] Clearly, the Co(II) species in the orange solution is a high-spin octahedral complex. No further characterization of this Co(II) species has been completed at the present time. As mentioned in the experimental section, exposure of the orange solution to oxygen brings about a rapid color change to deep red. Addition of $LiClO_4$ to the red solution affords crystalline $[Co(Pypep)_2]ClO_4 \cdot CH_3OH$ in high yield. Presumably the oxidation step is accompanied by the high-spin to low-spin transition.

(b) Redox Properties. The electrochemical behavior of $[Co(Pypep)_2]^+$ has been explored in Me_2SO, DMF, and methanol. Cyclic voltammograms of $[Co(Pypep)_2]^+$ in DMF at three different scan speeds are shown in Figure 3, and the half-wave potential ($E_{1/2}$) values are listed in Table IV. The Co(III) complex is reduced at relatively high negative potentials in all solvents. For example, in Me_2SO, when quoted vs aqueous SCE, and $E_{1/2}$ value of $[Co(Pypep)_2]^+$ is −0.70 V whereas that of $[Co(terpy)_2](ClO_4)_3$ is +0.25 V.[49] The +3 oxidation state of cobalt is thus stabilized by the peptide ligand **1** as compared to aromatic heterocyclic N-donor ligands like terpy. The peptide ligand **1** also provides maximum stabilization to Fe(III) among all the reported low-spin Fe(III) complexes with N-only donors.[21] In both cases, the preference for the +3 oxidation state exhibited by Pypep is largely due to the deprotonated amide N donor center which binds metal ions in higher oxidation states.[51]

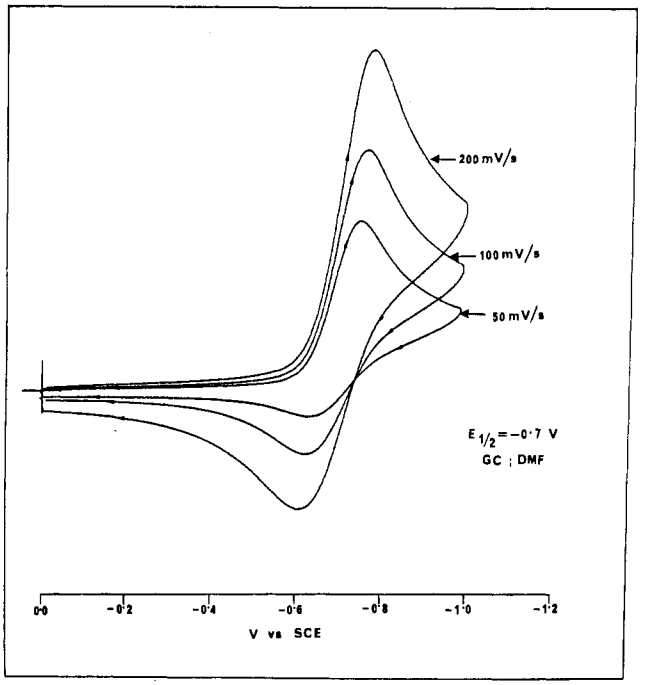

Figure 3. Cyclic voltammograms of **2** at three different scan speeds in DMF (glassy-carbon electrode, 0.1 M tetraethylammonium tetrafluoroborate).

Close inspection of Figure 3 reveals that the Co(II) species generated from one-electron reduction (evidenced by the variation of cathodic current height with scan speed) of $[Co(Pypep)_2]^+$ undergoes subsequent reaction or decomposition near the working electrode since a comparable amount of anodic current is detected only at a faster scan speed. The ratio of i_c/i_a is equal to 1 at scan speeds faster than 200 mV/s. The behaviors are practically identical on both glassy-carbon and Pt electrodes. Though Co(II) complexes in general are quite labile, Co(III) complexes with aromatic heterocyclic N-donor ligands like phen and terpy exhibit reversible electrochemical behavior. In fact, stable high-spin Co(II) complexes with such ligands have been known for a long time. With **1**, the situation is very different. The reduced species generated from $[Co(Pypep)_2]^+$ is unstable in all three solvents, and the instability increases as one goes from an aprotic solvent like DMF to a protic one like methanol.

Though we have not been able to isolate any Co(II) complex with **1** so far, a few comments regarding the instability of the reduced species from $[Co(Pypep)_2]^+$ can be made. Among the three donor centers of **1**, the imidazole and the pyridine nitrogens are expected to bind Co(II). The deprotonated amide nitrogen is, however, not a good ligand for cobalt in the +2 oxidation state.[54] Presumably, as $[Co(Pypep)_2]^+$ is reduced, the deprotonated amido nitrogen is detached from the metal center. The labile Co(II) complex might undergo further changes in coordination number and/or spin state. Ligand exchange can also occur. Any such

(43) Lever, A. B. P. In *Inorganic Electronic Spectroscopy*, 2nd ed., Elsevier: Amsterdam, 1984; pp 463–478.
(44) Morris, P. J.; Martin, R. B. *Inorg. Chem.* **1971**, *10*, 964.
(45) Figgis, B. N. In *Introduction to Ligand Fields*; Interscience: New York, 1966; p 247.
(46) $[Fe(Pypep)_2]^+$ displays the same band at 255 nm ($\epsilon \sim 12\,500\ M^{-1}\ cm^{-1}$).
(47) Reference 43; pp 480–489.
(48) Drago, R. S. In *Physical Methods in Chemistry*; Saunders: Philadelphia, 1977; Chapter XIII, p 497.
(49) Despite a considerable amount of electrochemical data on the Co(III) complexes of bpy, phen, and terpy,[50] direct comparison of their $E_{1/2}$ values with that of $[Co(Pypep)_2]^+$ was not possible since the reported experimental conditions varied to some extent. We have therefore measured the $E_{1/2}$ values of $[Co(bpy)_3](ClO_4)_3$, $[Co(phen)_3](ClO_4)_3$, and $[Co(terpy)_2](ClO_4)_3$ in Me_2SO using tetrabutylammonium perchlorate as the supporting electrolyte. A glassy-carbon electrode was used in such measurements. The $E_{1/2}$ values, quoted vs aqueous SCE at 25 °C are as follows: $[Co(phen)_3](ClO_4)_3$, +0.36 V; $[Co(bpy)_3](ClO_4)_3$, +0.29 V; $[Co(terpy)_2](ClO_4)_3$, +0.25 V.
(50) Maki, N.; Tanaka, N. In *Encyclopedia of Electrochemistry of the Elements*; Bard, A. J., Ed.; Marcel Dekker: New York, 1975; Vol. III, pp 43–210.
(51) Ligands containing deprotonated amide nitrogen(s) have been proved to be effective in stabilizing the +3 oxidation state of nickel[52] and copper.[53]
(52) (a) Haines, R. I.; McAuley, A. *Coord. Chem. Rev.* **1981**, *39*, 77. (b) Nag, K.; Chakravorty, A. *Coord. Chem. Rev.* **1980**, *33*, 87.
(53) Hathaway, B. J. *Coord. Chem. Rev.* **1983**, *52*, 87.
(54) Sigel, H.; Martin, R. B. *Chem. Rev.* **1982**, *82*, 385.

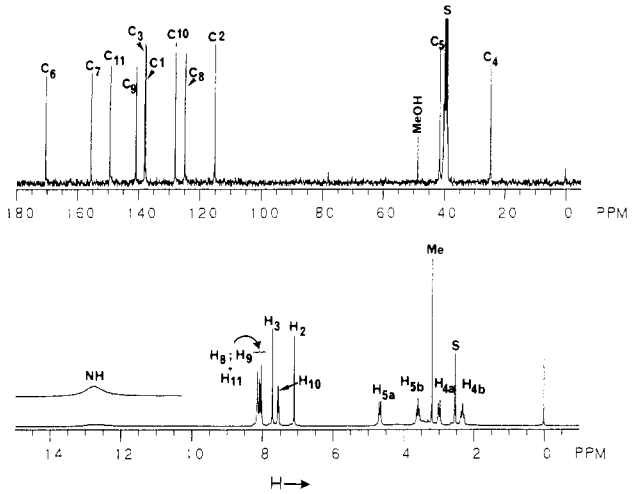

Figure 4. ^1H (lower trace) and ^{13}C (upper trace) NMR spectra (300 MHz, 296 K) of $[Co(Pypep)_2]ClO_4 \cdot CH_3OH$ in Me_2SO-d_6. Signal assignments (see Figure 7) are indicated.

alteration of the Co(II) species needs time. It is therefore possible to oxidize at least part of the Co(II) species back to $[Co(Pypep)_2]^+$ when the voltammetric scan speed is high and the direction of scan is switched at a point not far from the $E_{1/2}$ value (Figure 3). Otherwise, in solution, the reduced complex is transformed into some other Co(II) species that cannot be reoxidized to $[Co(Pypep)_2]^+$ electrochemically. It is interesting to note that the electronic absorption spectrum of an electrolyzed solution of **2** in methanol closely resembles the spectrum shown in Figure 2 as a broken line. Thus it appears that the "transformed" Co(II) species is the high-spin octahedral Co(II) complex, which is produced when 2 equiv of **1** are mixed with cobalt(II) acetate in methanol under anaerobic conditions. We believe that, in this complex, **1** is partially ligated to cobalt and the other coordination sites are occupied by solvent molecules.

The donor centers of BLM in M–BLMs have been assigned primarily on the basis of the preliminary crystal structure of the Cu(II) complex of P-3A, a putative peptide fragment of BLM.[55] Though binding of Cu(II) to peptide ligands enhances deprotonation of the amide group with concomitant coordination of the deprotonated amido nitrogen to the metal center, the same is not true for Fe(II) and Co(II).[54] Clearly, extension of the same set of donor centers (as observed in Cu(II)–P-3A) to different metals is an oversimplification. Even with the same metal in different oxidation states, the donor centers provided by BLM to the metal might vary. The present work points out the fact that in the various in vitro and vivo experiments, activation of M–BLMs with reductants and dioxygen is expected to produce metal-containing species with structures very different from what are predicted on the basis of spectroscopic data on M–BLMs with M in higher oxidation state(s). In particular, the results mentioned above suggest that even if the structure of Co(III)–BLM is known, it will be quite difficult to predict the structure of the photoreduced product especially when generated in presence of other chemical species.

(c) NMR Spectra. The ^1H and ^{13}C spectra of $[Co(Pypep)_2]ClO_4 \cdot CH_3OH$ in Me_2SO-d_6 are shown in Figure 4, and the spectral data are collected in Table V. For the sake of comparison, the ^1H and ^{13}C NMR data for PypepH (**1**) in the same solvent are also included in Table V. Since the two-dimensional NMR spectra were obtained with $[Co(Pypep)_2]ClO_4 \cdot H_2O$ (**2**), NMR data for **2** are also listed in Table V. In Figure 4 (and the following figures), the various hydrogen and carbon atoms of the complex have been labeled in accordance with Figure 1. The assignment of the various resonances in Figure 4 have been completed with the aid of ^1H–^1H and ^1H–^{13}C COSY results (vide infra) as well as APT and DEPT data.

(55) Itaka, Y.; Nakamura, H.; Nakatani, T.; Muraoka, Y.; Fuji, A.; Takita, T.; Umezawa, H. *J. Antibiot.* **1978**, *31*, 1070.

Table V. NMR Data for PypepH, $[Co(Pypep)_2]ClO_4 \cdot CH_3OH$, and $[Co(Pypep)_2]ClO_4 \cdot H_2O$ in Me_2SO-d_6 at 296 K[a]

^1H, δ (ppm from TMS)	^{13}C, δ (ppm from TMS)
PypepH[b]	
2.88 (t, J = 7.2 Hz, 2 H), 3.66 (q, J = 6.9 Hz, 2 H), 6.94 (s, 1 H), 7.60 (t, J = 6 Hz, 1 H), 7.68 (s, 1 H), 8.01 (t, J = 7.5 Hz, 1 H), 8.12 (d, J = 7.5 Hz, 1 H), 8.66 (d, J = 4.5 Hz, 1 H), 9.00 (t, J = 5.7 Hz, 1 H)	27.01, 39.02, 116.44, 134.93,[c] 121.88, 126.44, 137.76, 148.42, 150.05, 163.78
$[Co(Pypep)_2]ClO_4 \cdot MeOH$	
2.28 (t, J = 12 Hz, 1 H), 2.95 (d, J = 15 Hz, 1 H), 3.54 (t, J = 12 Hz, 1 H), 4.62 (d, J = 15 Hz, 1 H), 7.06 (s, 1 H), 7.51 (t, J = 6.3 Hz, 1 H), 7.67 (s, 1 H), 7.99 (t, J = 7.2 Hz, 1 H), 8.04 (t, J = 7.8 Hz, 1 H), 8.10 (d, J = 5.4 Hz, 1 H), 12.74 (s, br, 1 H)	24.68, 41.48, 115.07, 124.80, 127.98, 137.69, 138.01, 140.82, 149.30, 155.49, 170.50
$[Co(Pypep)_2]ClO_4 \cdot H_2O$	
2.32 (t, J = 12 Hz, 1 H), 2.99 (d, J = 15.3 Hz, 1 H), 3.58 (t, J = 12 Hz, 1 H), 4.66 (d, J = 15 Hz, 1 H), 7.10 (s, 1 H), 7.55 (t, J = 6 Hz, 1 H), 7.72 (s, 1 H), 8.03 (t, J = 7.2 Hz, 1 H), 8.08 (t, J = 7.8 Hz, 1 H), 8.14 (d, J = 5.7 Hz, 1 H), 12.78 (s, br, 1 H)	24.67, 41.49, 115.07, 124.81, 127.99, 137.68, 138.02, 140.83, 149.30, 155.48, 170.51

[a] Concentration: ~15 mM. [b] ^1H and ^{13}C NMR data for PypepH in $CDCl_3$ have been reported in ref 20. [c] The two carbon atoms C1 and C3 resonate at the same frequency.

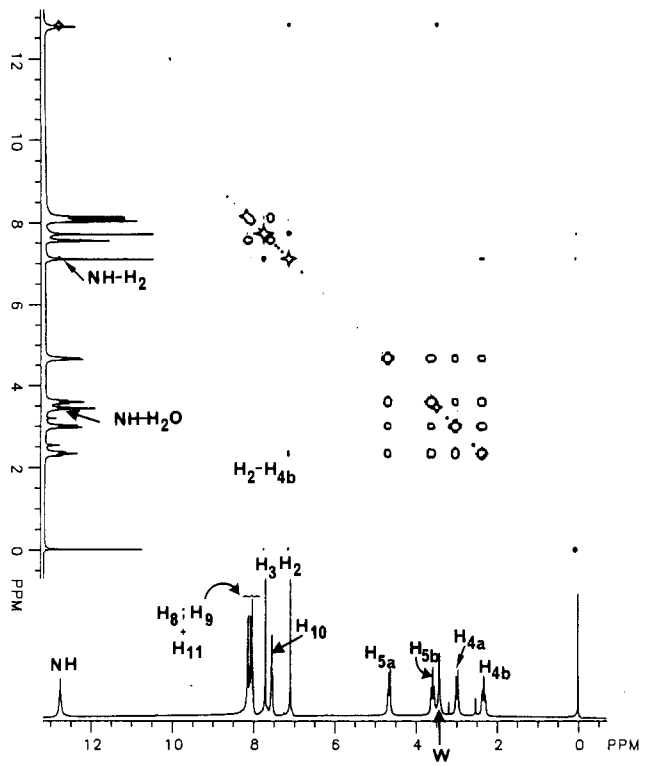

Figure 5. ^1H–^1H COSY spectrum of $[Co(Pypep)_2]ClO_4 \cdot H_2O$ (**2**) in Me_2SO-d_6. The peak due to H_2O is marked by W.

The most interesting feature of the ^1H NMR spectrum of $[CoPypep)_2]ClO_4 \cdot CH_3OH$ is the CH_2 region (1–5 ppm from TMS). In the ^1H NMR spectrum of **1**, the two CH_2 groups appear at 2.88 (a triplet) and 3.66 (a quartet) ppm. In the cobalt complex, however, the four H atoms resonate at four different positions (Figure 4, Table V). At 296 K, where the viscosity of the solution is high (Me_2SO freezes at 291 K), the four resonances give rise to a doublet, triplet, doublet, triplet (dtdt) pattern. The

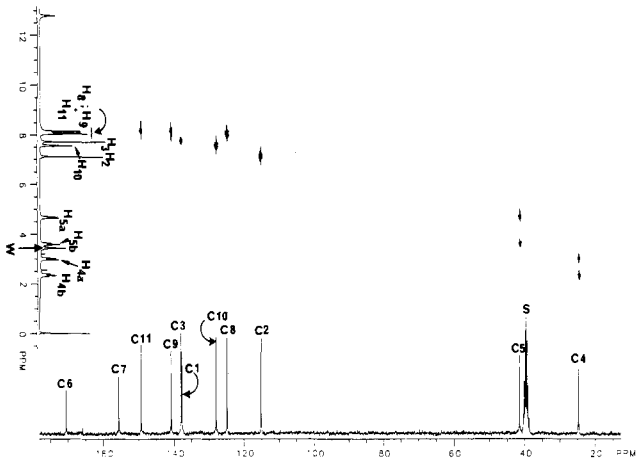

Figure 6. $^1H-^{13}C$ (J = 140 Hz) COSY spectrum of $[Co(Pypep)_2]ClO_4 \cdot H_2O$ (**2**) in Me_2SO-d_6. The peak due to H_2O is marked by W.

$^1H-^{13}C$ COSY spectrum (Figure 6) indicates that each CH_2 group affords a set of one doublet and one triplet, and the $^1H-^1H$ COSY spectrum (Figure 5) shows that all the four H atoms are coupled to each other. The "dtdt" pattern remains unchanged up to 353 K. Thus the four H atoms appear to be held in space quite rigidly in the chelate ring. The resolution improves significantly at 353 K, and additional structures are seen in the "dtdt" pattern. We have been able to measure the coupling constants for all the interactions among the four H atoms from the 353 K spectrum. The discussion on the solution structure of the Co(III) complex can however be completed without such detailed information, and hence the values of the coupling constants have been deposited as supplementary material (Table S6).

The CH_3 group of methanol in $[Co(Pypep)_2]ClO_4 \cdot CH_3OH$ gives rise to the peak at 3.15 ppm in the ^1H NMR spectrum. This assignment has been confirmed by external addition of CH_3OH. In case of $[Co(Pypep)_2]ClO_4 \cdot H_2O$, the protons of the water molecule resonate at 3.46 ppm. The peak disappers on addition of D_2O. Resonances for the two imidazole protons H2 and H3 have been assigned on the basis of their positions in the ^1H NMR spectra of other histidinato[56] and imidazole[35] complexes of cobalt. The NH peak shifts from 9.0 ppm in **1** to 12.74 ppm in the complex (Figure 4, Table V) presumably because the donation of electron density by N1 to cobalt results in deshielding of the H2′ proton. The NH peak is broad and disappears on addition of D_2O. Peak positions for the various pyridine protons have been assigned on the basis of chemical shifts, multiplicities, and the coupling constants of similar compounds.[57]

The ^{13}C NMR spectrum of $[Co(Pypep)_2]ClO_4 \cdot CH_3OH$ (Figure 4) exhibits 11 distinct resonances for the 11 carbon atoms of the ligand. The methanol carbon gives rise to a peak at 48.63 ppm. Assignments of the various carbon resonances rely in part on the APT and DEPT data. APT results clearly point out the resonances for the quaternary carbon atoms (C1, C6, and C7) and the two CH_2 carbons (C4 and C5). The peak corresponding to the carbonyl group (C6) moves from 163.78 ppm in the free ligand to 170.50 ppm in the complex as a result of coordination of the peptido nitrogen (N3) to cobalt. A similar shift of ^{13}C resonance of the carbonyl group due to coordination of peptide nitrogen to cobalt(III) has been reported.[26,56] Resonances of the various carbon atoms of the pyridine ring have been assigned on the basis of the ^{13}C NMR spectra of compounds like ethyl picolinate and picolinamide.[58]

Since variable-temperature NMR spectra of $[Co(Pypep)_2]ClO_4 \cdot S$ (S = CH_3OH or H_2O) indicate that the complex is very stable in solution and no dynamic rearrangement of the ligand framework is evident, we decided to check whether we could add hydrogen atoms to the framework shown in Figure 1 and come up with a solution structure of the complex that is supported by the homo- and heteronuclear COSY results. The $^1H-^1H$ and $^1H-^{13}C$ (J = 140 Hz) COSY spectra of $[Co(Pypep)_2]ClO_4 \cdot H_2O$ (**2**) in Me_2SO-d_6 solution are shown in Figures 5 and 6, respectively. The structure with the hydrogen atoms is shown in Figure 7. It must be emphasized here that, in Figure 7, we only intend to show the connectivity of the atoms and the proximity among the various hydrogens. No energy calculation has been completed, and the conformation of the ligand framework shown in Figure 7 is only approximate. Nevertheless, the COSY results discussed below corroborate Figure 7 very well, and we believe that Figure 7 is an adequate representation of the solution structure of the cobalt complex.

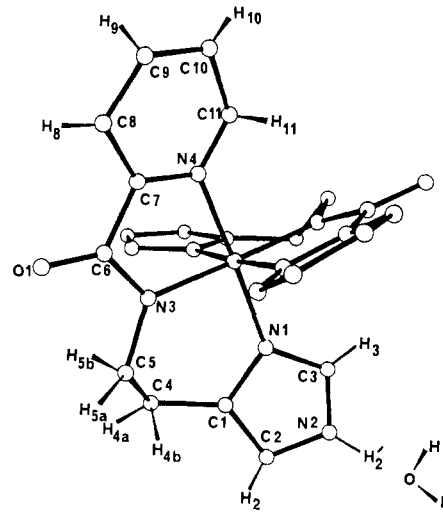

Figure 7. Proposed solution structure of $[Co(Pypep)_2]ClO_4 \cdot H_2O$ (**2**) in Me_2SO-d_6 as indicated by the NMR data (see text for details).

Close inspection of Figure 5 reveals that, in $[Co(Pypep)_2]^+$, the hydrogen atoms of the two CH_2 groups of the ligand are present as four distinct H atoms and they are all coupled to each other. Among them, H4b is also coupled to H2 of the imidazole moiety and is shown that way in Figure 7. A *vicinal* coupling constant value of 12 Hz prompted us to draw H5b *trans* to H4b. The approximate orientations of the remaining C–H bonds are based on the CH_2 *geminal* coupling constants of 14–15 Hz and *vicinal* coupling constants of 3–4 Hz. The two imidazole Hs (H2 and H3) are weakly correlated. Since the water molecule is coupled to H2, it appears that in Me_2SO-d_6 solution, the water molecule remains H-bonded to the NH group of the imidazole moiety (Figure 7).

The most important piece of information provided by Figure 6 is the fact that each CH_2 group of the ligand gives rise to a set of one doublet and one triplet in the ^1H NMR spectrum of the complex (Figure 4). Also, the $^1H-^{13}C$ COSY spectrum allows one to identify the resonances for C_2 and C_3. In addition, the long-range (J = 9 Hz) $^1H-^{13}C$ COSY spectrum (Figure S1, supplementary material) shows that C6 is coupled to both H5a and H5b.

Summary. The following points are the principal results and conclusions of this investigation.

(i) As part of a synthetic analogue approach to metallobleomycins, a cobalt(III) complex $[Co(Pypep)_2]ClO_4 \cdot H_2O$ (**2**) of the peptide ligand PypepH (**1**) has been isolated and structurally characterized. The spectroscopic properties of this orange-red cobalt complex have also been determined. The coordination sphere of cobalt in $[Co(Pypep)_2]^+$ is more symmetric than that proposed for Co(III)–BLM.

(ii) Formation of the orange cobalt(III) complex via aerobic oxidation of a mixture of cobalt(II) acetate and **1** parallels the formation of Co(III)–BLM though no *green* cobalt(III) species is observed.

(56) Hawkins, C. J.; Martin, J. *Inorg. Chem.* **1986**, *25*, 2146.
(57) Biemann, K. *Tables of Spectral Data for Structure Determination of Organic Compounds*; Springer-Verlag: West Berlin, 1983 (translated from German).
(58) *The Sadtler Handbook of Carbon-13 NMR Spectra*; Sadtler Research Laboratories: Philadelphia, 1984.

(iii) When $[Co(Pypep)_2]^+$ is reduced electrochemically, an unstable cobalt(II) species is formed. Rapid ligand reorganization in the first coordination sphere of the Co(II) center of this intermediate results in a high-spin octahedral cobalt(II) complex that can be independently synthesized by mixing cobalt(II) acetate and **1** (ratio 1:2) in degassed methanol.

(iv) The solution structure of the cobalt(III) complex has been proposed on the basis of one- and two-dimensional NMR data. Similar experiments with partially hydrolyzed Co(III)-BLM are expected to provide valuable information regarding the coordination structure of Co(III)-BLM.

Acknowledgment. This research was supported by a Faculty Research Grant and the donors of the Petroleum Research Fund, administered by the American Chemical Society, at the University of California and by NIH Grant GM 32690 at the University of Texas. We thank S. Brown for help in the synthesis of PypepH. Experimental assistance from S. Hudson and J. Loo is gratefully acknowledged.

Registry No. **2**, 112247-29-7; $[Co(Pypep)_2]ClO_4$, 112247-28-6; $[Co(Pypep)_2]BF_4$, 112247-30-0.

Supplementary Material Available: Crystal structure data for $[Co(Pypep)_2]ClO_4 \cdot H_2O$ (**2**) including thermal parameters for non-hydrogen atoms (Table S1), bond distances and angles in the anion (Table S2), positional parameters for the hydrogen atoms (Table S3), and unweighted least-squares planes of the cation (Table S4) and NMR data for **2** including coupling constants for the CH_2 protons of the ligand (Table S6) and the long-range (J = 9 Hz) ^1H-^{13}C COSY spectrum of **2** in Me_2SO-d_6 (Figure S1) (9 pages); observed and calculated structure factors (Table S5) (11 pages). Ordering information is given on any current masthead page.

Contribution from the Division of Chemical and Physical Sciences, Deakin University, Waurn Ponds 3217, Victoria, Australia, and Department of Inorganic Chemistry, University of Melbourne, Parkville 3052, Victoria, Australia

Electrochemical Reduction and Oxidation in Noncoordinating and Coordinating Solvents of Two Closely Related Binuclear Nickel(II) Complexes Containing either Sulfur or Oxygen Endogenous Bridging Centers

Alan M. Bond,*[1] Masa-aki Haga,[1,2] Ian S. Creece,[1] Richard Robson,[3] and Jenny C. Wilson[3]

Received April 27, 1987

Replacement of oxygen by sulfur as the endogenous bridging center of the nickel binuclear complexes $L(X)Ni_2(pz)$ (X = O, S; pz = pyrazolate; L = binucleating ligand component with peripheral *tert*-butyl substituents to solubilize the complexes in nonpolar solvents) leads to remarkable differences in their solution and redox chemistry. Whereas the diamagnetic planar complex $L(S)Ni_2(pz)$ shows no detectable specific solvent interaction in coordinating solvents such as dimethylformamide (DMF), the oxygen analogue forms the paramagnetic species $L(O)Ni_2(pz)(DMF)_2$ in solution from which the solid monosolvate $L(O)Ni_2(pz)(DMF)$ can be isolated. The reversible half-wave potentials, $E_{1/2}^r$, for the reduction processes

$$L(S)Ni_2(pz) \underset{-e^-}{\overset{+e^-}{\rightleftharpoons}} [L(S)Ni_2(pz)]^- \underset{-e^-}{\overset{+e^-}{\rightleftharpoons}} [L(S)Ni_2(pz)]^{2-}$$

as measured by voltammetric studies at platinum, gold, glassy-carbon, and mercury electrodes are separated by several hundred millivolts. In the noncoordinating nonpolar solvent dichloromethane, the reduced binuclear complexes are highly reactive. Nonspecific effects in polar solvents provide stability in the kinetic sense, whereas thermodynamic redox potentials are essentially solvent independent. By contrast, the two oxidation processes

$$L(S)Ni_2(pz) \underset{+e^-}{\overset{-e^-}{\rightleftharpoons}} [L(S)Ni_2(pz)]^+ \underset{+e^-}{\overset{-e^-}{\rightleftharpoons}} [L(S)Ni_2(pz)]^{2+}$$

have similar $E_{1/2}^r$ values and exhibit substantial specific solvent effects as does a further two-electron process to generate a highly reactive formally nickel(IV) complex $[L(S)Ni_2(pz)]^{4+}$. The solvent dependence of the cyclic voltammetry of the $L(O)Ni_2(pz)$ complex is substantially more complex than that for the sulfur analogue. Temperature and scan rate dependence as well as the presence of additional processes are observed in coordinating solvents that reflect the strong specific solvation terms associated with the coexistence of a range of $[L(O)Ni_2(pz)(solvent)_n]^m$ complexes (n = 0-4, m = 2+/+/0/-/2-) in coordinating solvents. Since the majority of voltammetric studies on nickel binuclear complexes have been conducted in solvents such as dimethylformamide or acetonitrile, the present information can be used to rationalize unexplained complexities previously reported on this important class of binuclear complex. Interestingly, the sulfur binuclear complex is more difficult to oxidize than the oxygen analogue, which is contrary to normal expectations. This illustrates the importance of the nature of the endogenous bridging centers in binuclear complexes.

Introduction

There has been extensive interest in the redox properties of binuclear transition-metal complexes of the type M_2L (M = metal, L = binucleating ligand(s)), particularly where M is copper or nickel. Binuclear complexes of this kind are of interest because the redox properties may be related to the multinuclear metal sites in metalloproteins,[4] particularly binuclear type III copper proteins.[5,6]

The majority of electrochemical studies on Cu_2L and Ni_2L complexes simply have reported half-wave potentials and whether the reduction and oxidation processes are reversible or irreversible. Furthermore, for reasons of solubility, almost all studies have been confined to coordinating solvents such as dimethylformamide (DMF) or acetonitrile (CH_3CN).[7-21] However, detailed elec-

(1) Deakin University.
(2) On leave from Mie University, Tsu, Mie, Japan.
(3) University of Melbourne.
(4) Sadler, P. J. *Inorg. Perspect. Biol. Med.* **1978**, *1*, 233.
(5) (a) Beinert, H. *Coord. Chem. Rev.* **1980**, *33*, 55. (b) Karlin, K. D.; Gultneh, Y. *J. Chem. Educ.* **1985**, *62*, 983.
(6) (a) *Copper Proteins and Copper Enzymes*; Lontie, R., Ed.; CRC: Boca Raton, FL, 1984, Vols. 1-3. (b) Solomon, E. D. *Copper Proteins*; Spiro, T. G. Ed.; Wiley: New York 1981; Chapter 2 and references therein.
(7) (a) Mazurek, W.; Bond, A. M.; O'Connor, M. J.; Wedd, A. G. *Inorg. Chem.* **1986**, *25*, 906 and references cited therein. (b) Nag, K.; Chakravorty, A. *Coord. Chem. Rev.* **1980**, *33*, 87. (c) Haines, R. I.; McAuley, A. *Coord. Chem. Rev.* **1981**, *39*, 77. (d) Addison, A. W. *Inorg. Nucl. Chem. Lett.* **1976**, *12*, 899. (e) Lintvedt, R. L.; Ranger, G.; Kramer, L. S. *Inorg. Chem.* **1986**, *25*, 2635.

0020-1669/88/1327-0712$01.50/0